文章编号：1001-9014(XXXX)XX-0001-10

DOI:10.11972/j.issn.1001-9014.XXXX.XX.001

Imaging simulation and analysis of attitude jitter effect on topographic mapping for lunar orbiter stereo optical cameras

CHEN Chen[1,2], TONG Xiao-Hua[1,2], LIU Shi-Jie[1,2*], YE Zhen[1,2], WU Hao[1,2], ZHANG Han[1,2]

(1. College of Surveying and Geo-Informatics, Tongji University, Shanghai 200092, China;
2. Shanghai Key Laboratory for Planetary Mapping and Remote Sensing for Deep Space Exploration, Tongji University, Shanghai 200092, China)

Abstract: The geometric accuracy of topographic mapping with high-resolution remote sensing images is inevitably affected by the obiter attitude jitter. Therefore, it is necessary to conduct preliminary research on the stereo mapping camera equipped on lunar orbiter before launching. In this work, an imaging simulation method considering the attitude jitter is presented. The impact analysis of different attitude jitter on terrain undulation is conducted by simulating jitter at three attitude angles, respectively. The proposed simulation method is based on the rigorous sensor model, using the lunar digital elevation model (DEM) and orthoimage as reference data. The orbit and attitude of the lunar stereo mapping camera are simulated while considering the attitude jitter. Two-dimensional simulated stereo images are generated according to the position and attitude of the orbiter in a given orbit. Experimental analyses were conducted by the DEM with the simulated stereo image. The simulation imaging results demonstrate that the proposed method can ensure imaging efficiency without losing the accuracy of topographic mapping. The effect of attitude jitter on the stereo mapping accuracy of the simulated images was analyzed through DEM comparison.

Key words: Lunar orbiter, attitude jitter, imaging simulation, stereo mapping camera, digital elevation model
PACS:

月球轨道器立体光学相机姿态颤振对地形测绘影响的成像仿真分析

陈 晨[1,2], 童小华[1,2], 刘世杰[1,2*], 叶 真[1,2], 吴 昊[1,2], 张 晗[1,2]

(1. 同济大学 测绘与地理信息学院,上海 200092;
2. 同济大学 上海市航天测绘遥感与空间探测重点实验室,上海 200092)

摘要:高分辨率遥感影像地形图的几何精度不可避免地受到轨道器姿态颤振的影响。因此,有必要在发射前对月球轨道器上搭载的立体测绘相机进行初步研究。提出了一种考虑姿态颤振的轨道器光学影像成像仿真方法。通过分别模拟三个姿态角的抖动,分析了不同姿态抖动对地形起伏的影响。所提出的模拟方法基于严格的成像模型,利用月球数字高程模型(DEM)和正射影像作为参考数据。在考虑姿态颤振的情况下,对月球立体测绘相机的轨道和姿态进行了仿真。根据轨道器在给定轨道上的位置和姿态生成二维模拟立体影像。利用DEM和仿真立体影像进行了实验分析。仿真成像结果表明,该仿真方法在保证成像效率的同时,又不损失地形制图的精度。通过DEM对比分析了姿态颤振对立体仿真影像制图精度的影响。

关 键 词:月球轨道器;姿态抖动;成像模拟;立体测绘相机;数字高程模型

中图分类号:O43 **文献标识码**:A

Received date: 2023-XX-XX, **revised date**: 2023-XX-XX **收稿日期**:2023- **修回日期**:2023-

Foundation items: Supported by the National Natural Science Foundation of China (42221002, 42171432); Shanghai Municipal Science and Technology Major Project (2021SHZDZX0100) and the Fundamental Research Funds for the Central Universities.

Biography: CHEN Chen (1996-), female, Shandong, doctor. Research area involves Geometric processing and application of optical images in deep space. E-mail: Cherry_chen@tongji.edu.cn.

* **Corresponding author**: E-mail: liusjtj@tongji.edu.cn

Introduction

Topographic mapping using stereo images obtained from orbiter optical cameras is a basic work in deep space exploration, to support engineering tasks and scientific research [1-2]. Chang'E-2 (CE-2) is China's second lunar orbiter, the stereo camera of it has achieved important scientific research achievements. China's Chang'E-7 (CE-7) lunar exploration orbiter will be equipped with a high-resolution stereo mapping camera to realize three-dimensional (3-D) mapping of the lunar surface and provide high-resolution spatial information for lunar morphology analysis and landing site selection. It is important to carry out pre-flight geometric analysis for the imaging system of a stereo-mapping camera. However, launching an experimental orbiter to verify the stability and accuracy of the imaging system is quite complex and expensive, and needs a long time of preparatory work. Therefore, it is critical to develop imaging simulation technology, which plays an important role in the verification and optimization of the platform and camera configuration.

Imaging simulation methods of orbiter cameras can be roughly divided into two categories: one is to use the ground object spectral database to simulate the imaging process by the empirical model[3-5]; another is to use the existing remote sensing image and terrain data by the photogrammetric simulation method, which makes up for the deficiency of empirical model. Compared to the research on imaging simulation of Earth orbiter cameras[6-15], the current research on lunar orbiter imaging is relatively less. Some studies focused on the three-line array CCD image, which can be simulated using the general collinear function based on the photogrammetric method[16]. Meanwhile, the BRDF effect of the lunar surface could be considered, and the gray value of the simulated image was corrected[17]. It must be mentioned that the existence of jitter in the actual imaging process needs to be considered in the simulation to expand and improve the imaging model[18-20].

High-resolution orbital stereo image mapping will be affected by the geometric quality of the image, and the effect of orbiter attitude jitter cannot be ignored. The production accuracy of the digital elevation model (DEM) in topographic mapping is declined markedly by the orbiter jitter[21-23]. Moreover, camera calibration in geometry preprocessing and the production of geometry products are also affected by orbiter attitude jitter[24-26]. The jitter analysis of Lunar Reconnaissance Orbiter (LRO) narrow angle camera (NAC) images acquired during Commissioning and early Primary Mapping Phases were presented, and a very regular pattern of approximately 10 m high ripples parallel to the cross-track direction was illustrated[23]. After that, it was found that problematic jitter seems to correlate with amplitudes of >1.5 pixels and frequencies at ~6 Hz[27].

The additional rotation angles between the satellite body coordinate system and the satellite orbit coordinate system are used to describe the platform vibration. During the imaging process of the stereo cameras on remote sensing orbiters, platform jitter causes continuous changes of roll, pitch, and yaw angle, which changes the looking direction of the camera, and then leads to the distortion of the image in the along-track direction and across-track direction. The simplified low-order polynomial model (SLPM) model can be used to describe the attitude changes of orbiters due to the relatively stable flight of orbiters in space. The essence of SLPM is to correct the deviation and drift error of the measurement data from the attitude measurement system. The systematic error of orbiter attitude angle can be simulated as a simplified LPM function at a certain imaging time. For the situation that only using the LPM cannot describe the orbiter attitude changes effectively, the fitting method of attitude jitter (e.g. polynomial function and sine function) is studied in view of the jitter error in attitude data, which can effectively simulate and eliminate the high-frequency and low-frequency errors in attitude data[28-30].

In summary, there have been many studies and analyses on Earth orbiter stereo mapping cameras, but is relatively little research on lunar orbiter imaging simulation. These researches focused on imaging simulation of three-line array cameras, with less research on stereo cameras. In addition, jitter was not considered and analyzed during the simulation process. In this paper, the imaging simulation of lunar orbiter stereo camera is to quantitatively analyze the impact of jitter on image and terrain construction, and provides a reference for the optimal configuration of high-resolution camera parameters of CE-7 orbiter platform. The stereo mapping camera is simulated on the basis of the characteristics and design parameters of the optical system. Finally, the corresponding stereo images are generated, meanwhile, the effect of orbiter attitude jitter on stereo image and stereo image mapping are simulated, and the feasibility of stereo mapping with camera image is verified. The effects of attitude jitter on terrain undulations are analyzed by simulating the jitter on different attitude angles separately.

1 Methodology

The procedure of the proposed simulation method is illustrated in Fig. 1. The imaging simulation method of the stereo mapping camera is conducted based on the rigorous imaging model construction. Firstly, in order to simulate the imaging procedure, the orbiter attitude, orbit, and camera parameters are introduced into the simulation model. Certain orbit parameters are determined by the range of DEM and Digital Orthophoto Map (DOM). Meanwhile, the effect of orbiter attitude jitter on stereo images is simulated. Then the mapping relationship between image points and ground points is established based on the collinearity equation. After obtaining the Lunar 3-D coordinates corresponding to pixel points, the coordinates of simulated image points on the DOM are calculated point by point. Finally, the corresponding stereo images are generated.

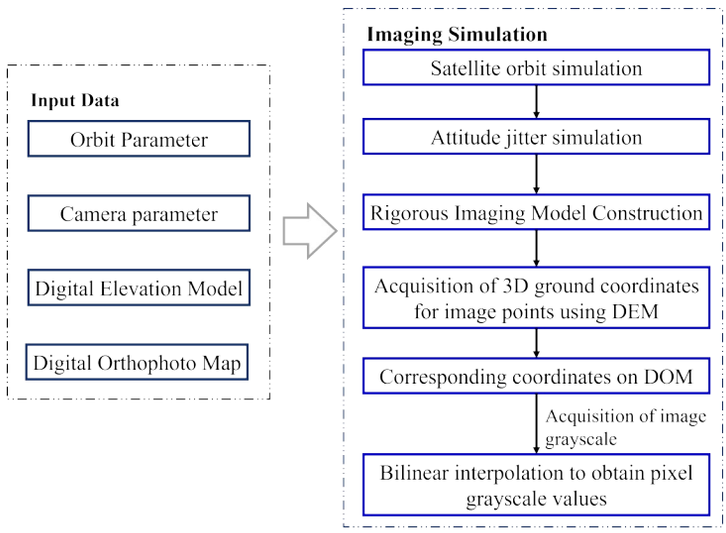

Fig. 1 Flowchart of imaging simulation for lunar stereo camera
图 1 月球立体相机成像仿真流程图

1.1 Rigorous imaging model

To find out the 3-D coordinates of lunar surface points from the image coordinates, it is necessary to establish the mapping relationship between the image coordinates and the lunar surface coordinates and thus to establish the rigorous imaging model of the camera, which is illustrated in Fig. 2.

The basic rigorous imaging model is based on the collinearity equation[31]. The collinearity equation of the stereo mapping camera at time t can be written as follows:

$$\begin{bmatrix} X \\ Y \\ Z \end{bmatrix}_{F_{Moon}} = \begin{bmatrix} X_S \\ Y_S \\ Z_S \end{bmatrix}_{F_{Moon}} + \lambda R_{camera}^{F_{Moon}} \begin{bmatrix} x \\ y \\ -f \end{bmatrix}. \tag{1}$$

where $\begin{bmatrix} x & y & -f \end{bmatrix}^T$ is the coordinate of image points in the camera coordinate system $Oc-XcYcZc$ which is shown in Fig. 2(b), f is the focal length of the camera; $\begin{bmatrix} X & Y & Z \end{bmatrix}_{F_{Moon}}^T$ is the coordinate of the 3-D points on the lunar surface corresponding to the image points in the lunar fixed coordinate system; $\begin{bmatrix} X_S & Y_S & Z_S \end{bmatrix}_{F_{Moon}}^T$ is the coordinate of the projection center of the camera in the lunar fixed coordinate system; $R_{camera}^{F_{Moon}}$ is the rotation matrix from camera coordinate system to lunar fixed coordinate system; λ is the projection coefficient (scale factor).

As shown in Fig. 2(b), the positions of the image point in the camera frame of the forward-looking camera and the backward-looking camera can be calculated by:

$$\begin{bmatrix} x \\ y \\ -f \end{bmatrix} = \begin{bmatrix} f*\tan(\alpha) - x_0 \\ (c_p - N/2)*ps - y_0 \\ -f \end{bmatrix}. \tag{2}$$

where ps is the pixel size of the stereo camera detector, α is the inclination angle of the stereo camera, c_p is the column position of point on the simulated image, N is

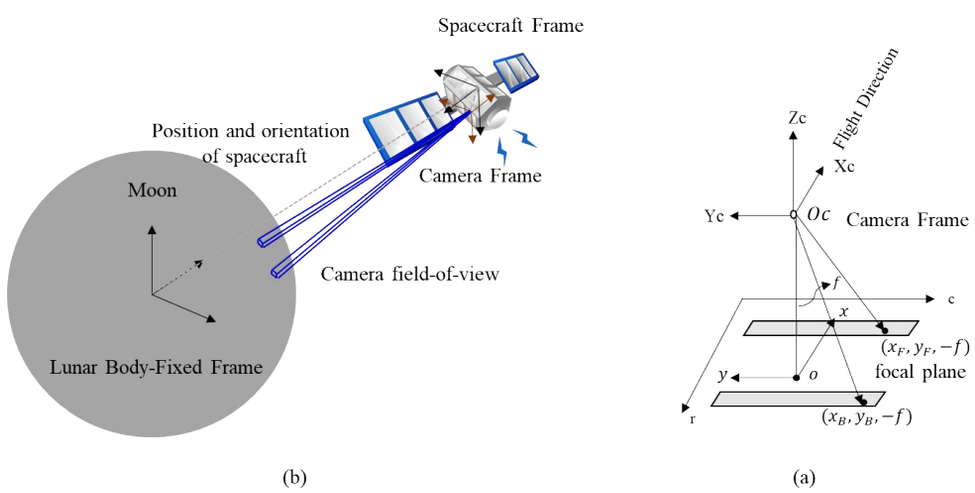

Fig. 2 Rigorous imaging model construction for lunar stereo cameras. :(a) mapping relationship between the camera frame and the lunar body-fixed frame; (b) Camera frame$Oc-XcYcZc$.
图 2 月球立体相机严格成像模型构建:(a)相机坐标系与月固坐标系的映射关系(b)相机坐标系 $Oc-XcYcZc$

number of columns of the stereo camera detector, (x_0, y_0) is coordinate of the principal point, f is the focal length of stereo camera.

Because the orbiter moves around the moon, the rotation matrix $R_{camera}^{F_{Moon}}$ in formula (1) is a function closely related to the orbiter position and sensor attitude, including the rotation angle of the imaging sensor relative to the satellite platform and the rotation angle of the satellite platform coordinate system relative to the lunar coordinate system. Therefore, the rotation matrix $R_{camera}^{F_{Moon}}$ can be expressed as the product of the rotation matrices among multiple coordinate systems:

$$R_{Camera}^{F_{Moon}} = R_{L_{Moon}}^{F_{Moon}} R_{S_{orbit}}^{L_{Moon}} R_{S_{body}}^{S_{orbit}} R_{camera}^{S_{body}}. \tag{3}$$

where $R_{camera}^{F_{Moon}}$is the rotation matrix from the camera coordinate system to the lunar fixed coordinate system, $R_{L_{Moon}}^{F_{Moon}}$ is the rotation matrix from lunar inertial coordinate system to lunar fixed coordinate system, $R_{S_{orbit}}^{L_{Moon}}$ is the rotation matrix from satellite orbital coordinate system to lunar inertial coordinate system, $R_{S_{body}}^{S_{orbit}}$ is the rotation matrix from satellite body coordinate system to satellite orbital coordinate system, which is the satellite attitude mentioned in 1.2, $R_{camera}^{S_{body}}$ is the rotation matrix from camera coordinate system to satellite body coordinate system.

1.2 Orbit and attitude jitter simulation model construction

The space position of the orbiter can be expressed by six orbit elements, namely, semi major axis $a$of orbiter orbit, eccentricity vector e, orbit inclination i, right ascension of ascending node Ω, argument of perigee ω, and true anomaly θ. The 3D coordinates $\begin{bmatrix} X_S & Y_S & Z_S \end{bmatrix}^T$of the orbiter in the lunar inertial coordinate system at a certain time are simulated by:

$$\begin{bmatrix} X_S \\ Y_S \\ Z_S \end{bmatrix} = \frac{a(1-e^2)}{1+\mathrm{e}\cos\theta} \begin{bmatrix} \cos\Omega\cos(\omega+\theta) - \sin\Omega\sin(\omega+\theta)\cos i \\ \sin\Omega\cos(\omega+\theta) - \cos\Omega\sin(\omega+\theta)\cos i \\ \sin(\omega+\theta)\sin i \end{bmatrix}. \tag{4}$$

Although there are different factors leading to the orbiter jitter, such as orbiter attitude adjustment, solar wing rotation and so on. However, the platform vibration can be approximately regarded as sinusoidal jitter because of its periodicity or similar to periodicity[32]. The model of attitude jitter on the orbiter is expressed as a simple sine function:

$$F_\alpha(t) = A_i \sin(2\pi f_i t + p_i). \tag{5}$$

where α is the attitude jitter angle (roll, pitch, and yaw angle) between the satellite body coordinate system and the satellite orbit coordinate system, t is the imaging time, A_i, f_i, p_i are the amplitude, frequency and phase of attitude jitter component, respectively.

1.3 Stereo image simulation model

A stereo camera system typically has two cameras that capture images from different angles of the same scene. Firstly, based on the imaging range of the image to be simulated, the imaging time t of the forward-looking camera and the backward-looking camera that cover that range can be determined. Afterwards, the rigorous imaging model of stereo mapping camera can be obtained by transforming collinearity equation in formula (1):

$$\begin{aligned} X &= X_S + (Z - Z_S)\frac{R_{(1,1)}x + R_{(1,2)}y - R_{(1,3)}f}{R_{(3,1)}x + R_{(3,2)}y - R_{(3,3)}f} \\ Y &= Y_S + (Z - Z_S)\frac{R_{(2,1)}x + R_{(2,2)}y - R_{(2,3)}f}{R_{(3,1)}x + R_{(3,2)}y - R_{(3,3)}f} \end{aligned}. \tag{6}$$

where $R_{(i,j)}$ (i=1,2,3; j=1,2,3) is the elements of R matrix at ith row and jth column.

The 3D coordinates of points (X, Y, Z) in formula (6) are calculated as follows: (1) take an approximate elevation value Z_0; (2) substitute the $(x, y, -f)$ and Z_0 into the formula (6) to calculate the approximate value of ground plane coordinate (X_0, Y_0); (3) use (X_0, Y_0) and reference DEM to calculate elevation Z_1; (4) repeat step (2) and (3) until the difference between $(X_{i+1}, Y_{i+1}, Z_{i+1})$ and (X_i, Y_i, Z_i) is less than $10^{-6}m$. The process is shown in Fig. 3.

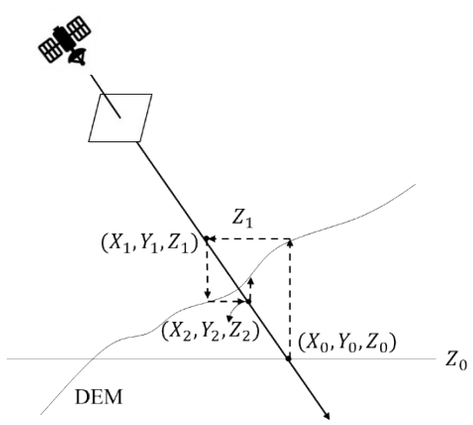

Fig. 3 Process for the calculation of 3-D coordinate of points in the lunar fixed coordinate system.
图3 像点对应的月固坐标系下的三维坐标的计算过程

The 3D coordinates of the ground objects in the lunar fixed coordinate system can be transformed into coordinates in the geodetic coordinate system with the same projection method as DOM. Then, according to the coordinates in the geodetic coordinate system, the position (i. e. the number of rows and columns) of the point on the DOM is calculated by the following formula:

$$\begin{bmatrix} Line \\ Sample \end{bmatrix} = \begin{bmatrix} \dfrac{x - x_0}{\Delta x} \\ \dfrac{y - y_0}{\Delta y} \end{bmatrix}. \tag{7}$$

where $(Sample, Line)$is the coordinate of corresponding pixels in DOM, (x_0, y_0) is the coordinates of the point in the upper left corner of DOM, Δx and Δy are the spatial resolution of DOM in the two projection directions respectively. According to the position of the point on the

DOM, the bilinear interpolation algorithm is used to obtain the pixel gray value of the simulation image corresponding to the point from the DOM.

With the above steps, the simulated image is generated pixel by pixel as follows: first, based on the collinearity equation, the rigorous imaging model in 1.1 was constructed; secondly, according to the existing camera and orbit parameters, orbit and attitude jitter simulation model of the stereo camera as described in Section 1.2; Then, the stereo image simulation model from image point to lunar surface is established by transforming into the form in 1.3; After that, input the DEM and use equation (6) to iteratively obtain the 3-D coordinates (X, Y, Z) corresponding to each pixel on the image, and calculate the coordinates of each image point on the DOM to obtain the image grayscale; finally, generate the corresponding stereo images and obtain the results in section 2.2.

1.4 Theoretical derivation of the influence of attitude jitter on stereo mapping accuracy

The elevation error of the along-track stereo camera is mainly related to the relative error of the forward-looking and backward-looking images in the along-track direction[33]. As shown in Fig. 4, for the point P_1 on the forward image, its projection error in the along-track direction is ΔE_1, for point P_2 on the backward image, and its projection error in the along-track direction is ΔE_2. The elevation error can be estimated according to the positioning error of forward and backward images in the along-track direction:

$$\Delta H \approx \frac{\frac{\Delta E_1 + \Delta E_2}{2}}{\tan(\frac{\delta}{2})}. \tag{8}$$

$$\Delta E_i = H^*(tan(\alpha + F_\alpha(t)) - \tan(\alpha)), i = 1,2. \tag{9}$$

where, ΔH is the elevation error, δ is the intersection angle of forward and backward images, α is the inclination angle of the stereo camera, $F_\alpha(t)$ is the model of attitude jitter in formula (5). It can be seen from the formula (8) that the greater the difference between the positioning accuracy of forward image and backward image by the attitude jitter, the greater the impact on the elevation accuracy.

2 Experiment and discussions

2.1 Experimental design

Chang'e 4 (CE-4) is the lunar probe of China, that successfully landed in the Von Kármán crater of the South Pole Aitken (SPA) on the far side of the Moon. The input DEM and orthomap for simulation were constructed using LRO NAC images by Arizona State University in the landing site of CE-4[1], which are shown in Fig. 5. The target simulation area for simulated images is illustrated by the red box in Fig. 5. The resolution of the DEM and orthophoto map are 5 m and 1.5 m respectively.

The stereo camera system in the imaging simulation experiment involves two cameras that are the forward-looking camera and the backward-looking camera. The parameters of the simulated stereo camera are shown in Table 1. These two cameras are designed to obtain along-track stereo imagery. The inclination angles of the forward-looking camera and backward-looking camera are 24.5° and -6.5°. The focal length for the simulated stereo camera is 0.7 m, and the pixel size is 7 um. The orbit of the stereo camera system has an altitude of 200 km above the surface of the moon, and the orbit shape is circular.

2.2 Stereo image simulation results

The imaging simulation results are shown in Fig. 6. Fig. 6(a) is the simulated forward-looking image, and Fig. 6(b) is the simulated backward-looking image. Image matching between the orthophoto image used in the imaging simulation and the simulated stereo images is performed to generate control points. The elevation of the control points is obtained from the reference DEM. The inverse process of the simulation process was carried out to calculate the image points of the control points, and

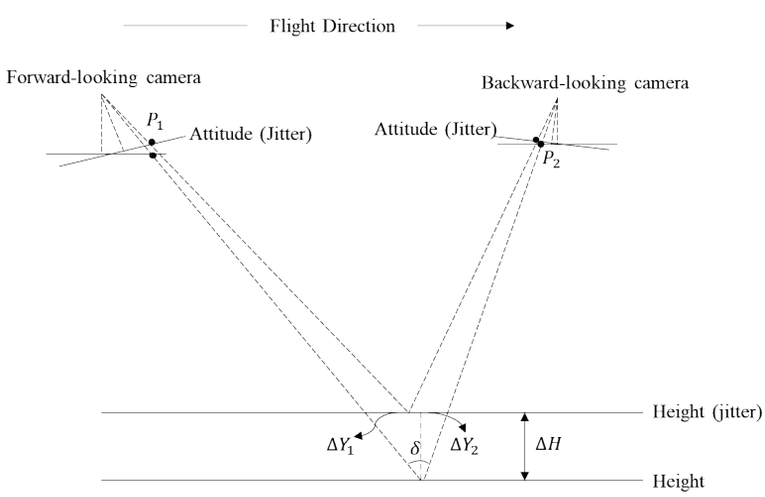

Fig. 4 The impact of attitude jitter on stereo intersection.
图 4 姿态颤振对立体交会的影响

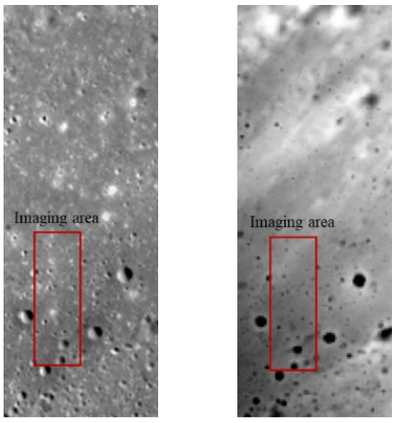

(a) (b)

Fig. 5 Input data of the simulation: (a) reference DOM; (b) reference DEM; the red box represents the imaging area of the simulated image
图5 仿真输入数据:(a)参考DOM;(b)参考DEM;红框内是仿真影像成像区域

Table 1 Parameters of stereo camera in imaging simulation
表1 仿真中的立体相机参数

Parameters	Value
Inclination angle	Forward view: 24.5° Backward view: −6.5°
Pixel size	7 um
Focal length	0.7 m
Orbit altitude	200 km
Orbit shape	Circle
Orbit type	Polar orbit
Ground resolution	2 m

the re-projection residuals were computed by the difference between the measured image points and the calculated image points. There are 14007 and 36490 control points of the stereo images after matching. The accuracy of the imaging simulation method is evaluated by the statistics of residuals, which are shown in Table 2. The average and standard deviation values of the re-projection residuals are less than 0.5 pixels, which reflects the effectiveness and accuracy of the simulation method.

Subsequently, DEM is generated by the simulated images to verify the geometric accuracy. Fig. 7(a) is the reference DEM, and Fig. 7(b) is the DEM generated from simulated images. Then, the profiles of DEM and reference DEM are analyzed. The profiles drawn on DEMs are shown in Fig. 7, and the elevation difference along the profiles between DEMs is shown in Fig. 8. The elevation on the simulated DEM along the profiles is almost the same with the reference DEM, while small difference exists at the bottom of the crater. This small elevation difference may be due to different methods of constructing DEM. Unlike the construction method of the reference DEM[1], the method used to construct DEM from simulated images is: 1) generating the rational polynomial coefficients (RPCs) from the rigorous imaging model; 2) constructing the DEM based on the SGM dense matching algorithm. Due to different methods of producing DEM, it may also lead to elevation difference of DEMs.

The elevation difference between the reference DEM and the simulated DEM is calculated to validate the positioning accuracy of the simulated images. There are 2897950 plane points generated evenly distributed on DEM, and the elevation values of two DEMs based on the

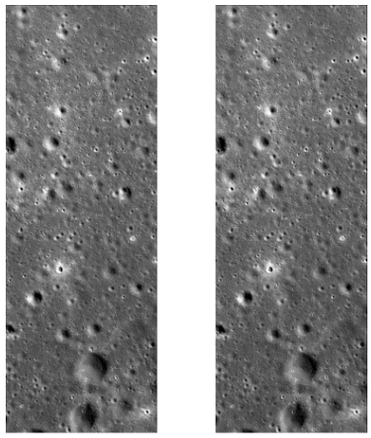

(a) (b)

Fig. 6 Simulated images: (a) forward-looking image; (b) backward-looking imageTable 2 Statistical values of re-projection residuals for control points
图6 仿真影像:(a)仿真的前视影像;(b)仿真的后视影像

表2 控制点反投影残差的统计值

Statistical value	Average/*pixel*		Standard Deviation/*pixel*	
	Sample	Line	Sample	Line
Backward-looking image	−0.073	−0.069	0.218	0.299
Forward-looking image	0.066	0.021	0.366	0.382

position of the same plane point could be obtained. The

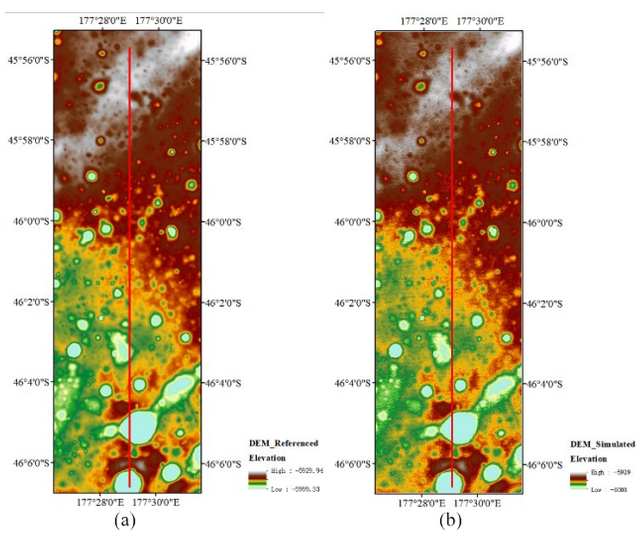

(a) (b)

Fig. 7 Analysis of the simulation method: (a) reference DEM; (b) DEM generated from simulated images; the red lines represent the profile on the DEMs
图7 仿真方法分析:(a)参考DEM;(b)由仿真的立体影像生成的DEM;红线代表DEM上的剖面线

histogram of the elevation differences from all plane points is shown in Fig. 9. The average and standard deviation of the elevation differences are -0.151 m and 0.759 m, respectively. The results show that the eleva-

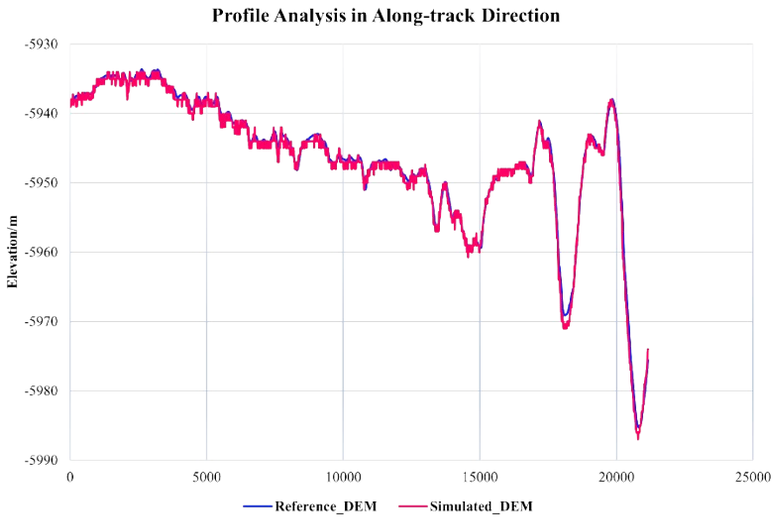

Fig. 8 Profile analysis of the reference DEM and the DEM generated from simulated stereo images
图8 参考DEM和仿真立体影像生成的DEM的高程剖面分析

tion difference is mostly within 2 m, which obeys normal distribution. The histogram statistical data shows that the images of lunar orbiter stereo camera were simulated by the imaging simulation model precisely, fully verifying the accuracy of the simulation process. Moreover, this embodies the positioning accuracy of the simulation images, proving that the stereo images generated from imaging simulation can construct DEMs that are close to the reference DEM.

2.3 Simulation and analysis of the influence of attitude jitter on mapping accuracy

To analyze the effect of attitude jitter of lunar orbiter on the imaging of stereo mapping camera, several groups of simulation experiments were set up to analyze the influence of attitude angle of lunar orbiter on terrain undulation. The frequency of 0.6 Hz refers to the jitter frequency of ZY-3 image[22]. The amplitude and frequency of the jitter model are 3 arc seconds (arc-sec) and 6 Hz, which reference the jitter detected from the LROC NAC jitter image[23].

For the along-track stereo image, the elevation error is mainly related to the jitter in the along-track direction, which is determined by the pitch angle. Therefore, a low-frequency jitter is added to the pitch angle. The DEMs are generated using the stereo images simulated by the attitude jitter model, as shown in Fig. 10(a) and (b). The differential DEM shown in Fig. 10(c) and (d) are produced by the difference between the reference DEM in Fig. 10(a) and the DEM in Fig. 10(b) so as to separate the influence of jitter.

The red line drawn in Fig. 8(d) represents the profile line, and its elevation is illustrated in Fig. 11. When the amplitude is 3 arc-sec, the maximum terrain undulation can be calculated to be about 10.75 m by for-

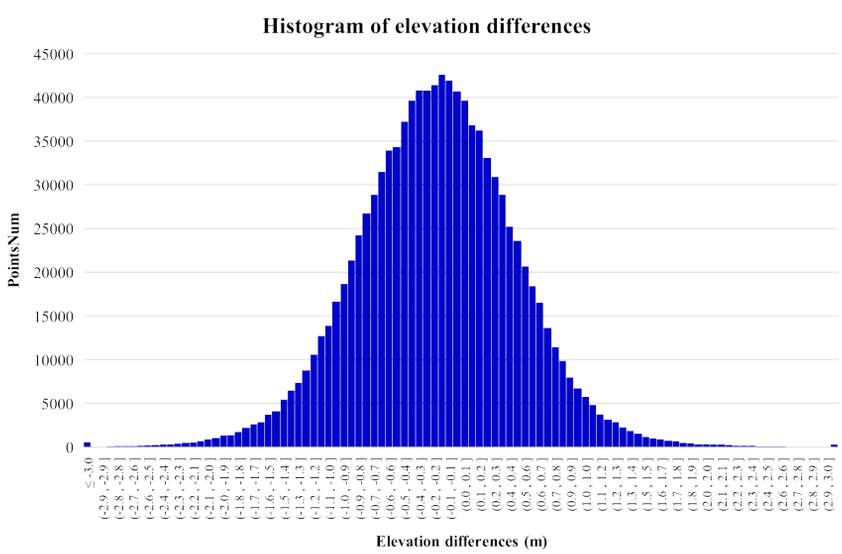

Fig. 9 Histogram of elevation value difference of the reference DEM and the DEM generated from simulated stereo images
图9 参考DEM和仿真立体影像生成的DEM的高程差直方图

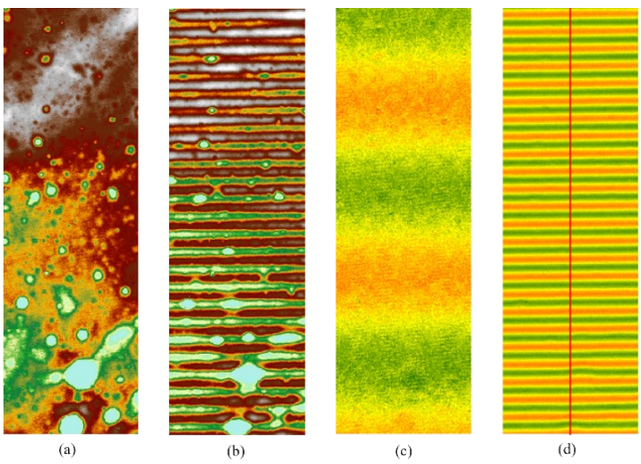

Fig. 10 Analysis of jitter added on pitch angle: (a) DEM with jitter (3", 0.6HZ); (b) DEM with jitter (3 arc-sec, 6HZ); (c) differential DEM of reference DEM and (a); (d) differential DEM of reference DEM and (b);

图 10 仿真中俯仰角上添加颤振的地形分析:(a)颤振 DEM(3 arc-sec,0.6 Hz);(b)颤振 DEM(3 arc-sec,6 Hz);(c)参考 DEM 和(a)中 DEM 的差分 DEM;(d)参考 DEM 和(b)中 DEM 的差分 DEM

mula (8). By comparing with the Fig. 11, it is found that the results are consistent. It can be shown that when the amplitude of jitter is 3 arc-sec, the maximum topographic relief can be up to more than 10 m. According to the results in the work of Mattson et al. [23], when the amplitude and frequency of the jitter model are 3 arc seconds (arc-sec) and 6 Hz, there also exists a very regular pattern of approximately 10 m high ripples parallel to the cross-track direction on the DEM. This also demonstrates the accuracy of jitter simulation results.

Figure 12 shows the DEM constructed when jitter is added at the yaw angle and Figure 13 shows the DEM constructed only when jitter is added at the roll angle. By analyzing the experimental results, with the increase of frequency, there are more jitter "stripes" on DEM. When adding the same amplitude and frequency jitter, the influence of yaw angle jitter on DEM constructed by stereo camera image is not obvious compared pitch angle. When adding the same amplitude and frequency jitter, the influence of roll angle jitter on DEM constructed by stereo camera image is negligible.

3 Conclusions

In this paper, an imaging simulation method of the lunar orbiter stereo camera is presented considering attitude jitter. The imaging simulation is conducted on the basis of the characteristics and design parameters of the stereo mapping camera, which can simulate the stereo images without and with attitude jitter. Finally, the simulated stereo images were generated. To verify the simulation method and analyze the effect of orbiter attitude jitter, DEMs without and with jitter were conducted by the simulated images.

The main conclusions are as follows: (1) This method can generate the corresponding stereo images according to the position and attitude of the orbiter with the given orbit parameters; (2) The stereo imaging results show that this method can ensure the imaging efficiency without losing the accuracy of the original digital elevation model; (3) The DEM results show that the elevation difference between the DEM generated by the simulation image and the reference DEM is mostly within 2 m, which demonstrates the positioning accuracy of the simulation images; (4) The influence of orbiter attitude jitter on stereo mapping camera image is able to simulated, which is reflected in the terrain undulation by stereo mapping; (5) When adding the same amplitude and frequency jitter, the influence of yaw angle jitter on DEM constructed by stereo camera image is not obvious compared pitch angle, the influence of roll angle jitter on DEM constructed by stereo camera image is negligible. The experiments prove that the proposed imaging simulation method provides a reference for the optimal configuration of high-res-

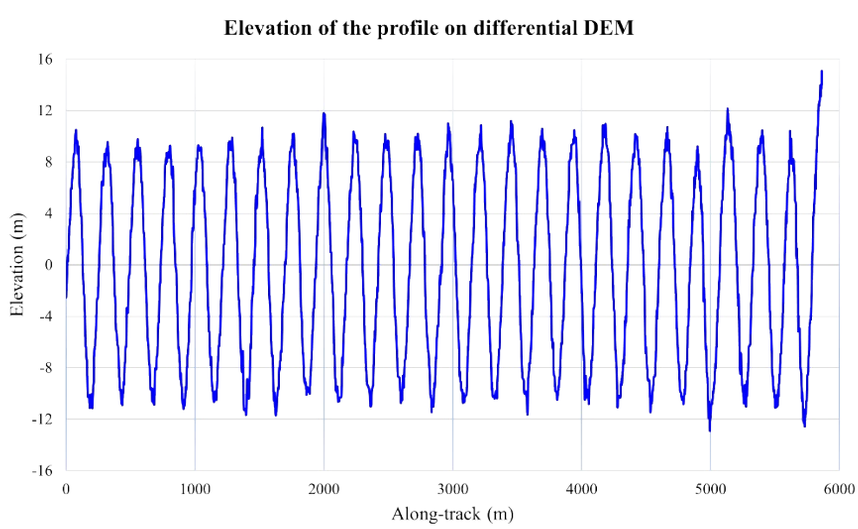

Fig. 11 Elevation of profile drawn on differential DEM

图 11 差分DEM上的剖面高程

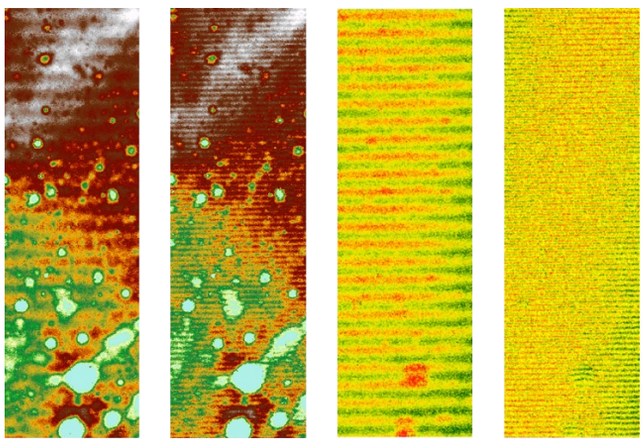

Fig. 12 Analysis of jitter added on yaw angle: (a) DEM with jitter (3", 0.6HZ); (b) DEM with jitter (3 arc-sec, 6HZ); (c) differential DEM of reference DEM and (a); (d) differential DEM of reference DEM and (b);
图 12 仿真中偏航角上添加颤振的地形分析: (a)颤振 DEM(3 arc-sec,0.6 Hz);(b)颤振 DEM(3 arc-sec,6 Hz);(c)参考 DEM 和(a)中 DEM 的差分 DEM;(d)参考 DEM 和(b)中 DEM 的差分 DEM

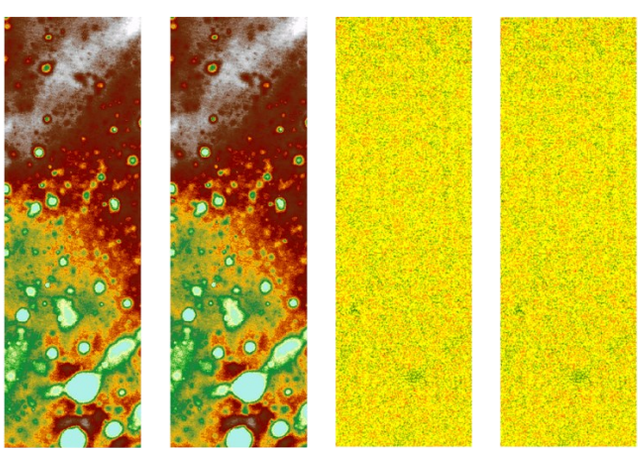

Fig. 13 Analysis of jitter added on roll angle: (a) DEM with jitter (3", 0.6HZ); (b) DEM with jitter (3 arc-sec, 6HZ); (c) differential DEM of reference DEM and (a); (d) differential DEM of reference DEM and (b);
图 13 仿真中滚转角上添加颤振的地形分析: (a)颤振 DEM(3 arc-sec,0.6 Hz);(b)颤振 DEM(3 arc-sec,6 Hz);(c)参考 DEM 和(a)中 DEM 的差分 DEM;(d)参考 DEM 和(b)中 DEM 的差分 DEM

olution camera parameters from the lunar satellite platform.

References

[1] Henriksen M R, Manheim M R, Burns K N, *et al*. Extracting accurate and precise topography from LROC narrow angle camera stereo observations[J]. *Icarus*, 2017, **283**: 122-137.
[2] Kokhanov A A, Karachevtseva I P, Zubarev A E, *et al*. Mapping of potential lunar landing areas using LRO and SELENE data[J]. *Planetary and Space Science* , 2017, **162**: 179-189.
[3] Zanoni V, Stanley T, Blonski S, *et al*. Satellite Hyperspectral Imaging Simulation[J]. *International Symposium on Spectral Sensing Research*, 1999.
[4] Qiu X F, Zhao H J, Jia G R, *et al*. Atmosphere and Terrain Coupling Simulation Framework for High-Resolution Visible-Thermal Spectral Imaging over Heterogeneous Land Surface[J]. *Remote Sensing*, 2022, **14**(9): 2043.
[5] Li M X, Jiang G W, Zhang R. The Semi-Physical Simulation System Designed for Space Optical Remote Sensing Based on 6-DOF Motion Platform[C]// Proceedings of the 2016 International Forum on Management, Education and Information Technology Application, 2016. pp705-709.
[6] Ebner H, Kornus W, Strunz G, Hofmann O, Mueller F. A simulation study on point determination using MOMS-02/D2 imagery[J]. *Photogrammetric Engineering & Remote Sensing*, 1991, **57**(10): 1315-1320.
[7] Li R, Zhou G, Schmidt N J, Fowler C, Tuell G. Photogrammetric processing of high-resolution airborne and satellite linear array stereo images for mapping applications[J]. *International Journal of Remote Sensing*, 2002, **23**(20): 4451-4473.
[8] Jiang W S, Zhang J Q, Zhang Z X. Simulation of three-line CCD satellite images from given orthoimage and DEM [J]. Geomatics and Information Science of Wuhan University, 2002(04): 414-419.(江万寿,张剑清,张祖勋.三线阵CCD卫星影像的模拟研究[J].**武汉大学学报(信息科学版)**),2002,(04):414-419.
[9] Xu Y. Research on Imaging Mechanism and Image Simulation of Alrborne Three-line Scanner [D]. Wuhan University, 2004.(许宇.机载三线阵CCD传感器成像机理及影像模拟研究[D].武汉大学, 2004.
[10] Wang J R, Li J, Zhao F, Liu W. On the Simulation of Three-Line-Array CCD Satellite imagery[J]. Geomatic Science and Engineering, 2008.(王建荣,李晶,赵斐,刘薇.三线阵CCD卫星影像的模拟[J].**测绘科学与工程**), 2008.
[11] Luo S, Zhang R, Jiang T, Jiang G W, Wang X. Simulation of High Resolution Linear CCD Satellite Images of the City Area[J]. Journal of Geomatics Science and Technology, 2011, **28**(02): 125-128+133.(罗胜,张锐,姜挺等.城市区域高分辨率线阵CCD卫星影像模拟[J].**测绘科学技术学报**),2011,**28**(02):125-128+133.
[12] Tang X M, Zhang G, Huang W C, *et al*. Simulation method of LEO satellite image: CN201210492407.1[P].2013-02-26.(唐新明,张过,黄文超,等.低轨卫星影像仿真方法:CN201210492407.1[P], 2013.
[13] Xie J H, Liu M J, Qiu Z G, Zhao K, Zhang C L. Ray-tracing simulation on imagery of satellite borne linear-array CCD camera based on cluster architecture. [J]. *Science of Surveying and Mapping*, 2015, **40**(11): 150-154.
[14] Yue Q X, Tang X M, Gao X M. Imaging Simulation of Sub-meters Satellite TDI CCD Camera for Surveying and Mapping[J]. *Geomatics and Information Science of Wuhan University*, 2015, **40** (03): 327-332.
[15] Mo D L, Zhang Y S, Wang T, Zhang Y. Imaging Simulation of Airborne Linear Whiskbroom Camera [J]. Acta Optica Sinica, 2018, **38** (07): 336-345.(莫德林,张永生,王涛等.航空线阵摆扫式相机成像仿真[J].**光学学报**),2018,**38**(07):336-345.
[16] Wang X Y, Yin M, Wang J R, *et al*. On the Simulation Technique in Lunar Photogrammetry [J]. Geomatic Science and Engineering, 2008, (3): 31-35.(王新义, 尹明, 王建荣, 等.月球摄影测量仿真技术[J]. **测绘科学与工程**), 2008, (3): 31-35.
[17] Li Q Z, Zhang W M, Yan G J, *et al*. Simulation of Three-line CCD Satellite Images of the Moon[J]. Journal of Beijing Normal University (Natural Science), 2007, **043**(003): 298-302.(李巧枝, 张吴明, 阎广建等.月球卫星三线阵CCD影像模拟[J].**北京师范大学学报(自然科学版)**), 2007, **043**(03): 298-302.
[18] Liu H Q, Ma H M, Jiang Z H, *et al*. Jitter detection based on parallax observations and attitude data for Chinese Heavenly Palace-1 satellite[J]. *Opt. Express*, 2019, **27**(2): 1099-1123.
[19] Zhang Z, Iwasaki A, Xu G. Remote Sensing Satellite Jitter Detection Based on Image Registration and Convolutional Neural Network Fusion[C]// IGARSS 2019 - 2019 IEEE International Geoscience and Remote Sensing Symposium, Yokohama, Japan, 2019, pp10035-10038.
[20] Ye Z, Xu Y S, Zheng S Z, *et al*. Resolving time-varying attitude jitter of an optical remote sensing satellite based on a time-frequency analysis[J]. *Opt. Express*, 2020, **28** (11): 15805-15823.
[21] Cao J S, Yang B, Wang M. Jitter compensation of ZiYuan-3 satellite imagery based on object point coincidence[J]. *International Journal of Remote Sensing*, 2019, **40**(16): 6116-6133.
[22] Wang M, Zhu Y, Jin S Y, *et al*. Correction of ZY-3 image distortion caused by satellite jitter via virtual steady reimaging using attitude data [J] *ISPRS Journal of Photogrammetry and Remote Sensing*, 2016, **119**: 108-123.
[23] Mattson S S, Robinson M, McEwen A, *et al*. Early Assessment of

Spacecraft Jitter in LROC-NAC[C]// 41st Lunar and Planetary Science Conference. The Woodlands, Texas, 2010.
[24] Wang M, Tian Y., Cheng Y F. Development of On-orbit Geometric Calibration for High Resolution Optical Remote Sensing Satellite[J] *Geomatics and Information Science of Wuhan University*, 2017, **42**(11):1580-1588.
[25] Zhang H, Xie B R, Liu S J, *et al*. Detection and Correction of Jitter Effect for Satellite TDICCD Imagery[C]// The International Archives of the Photogrammetry, Remote Sensing and Spatial Information Sciences, XLIII-B1-2022, pp79 - 84.
[26] Kocaman S, Gruen A. Orientation and self-calibration of ALOS PRISM imagery [J]. *Photogrammetric Record*, 2010, **23**(123): 323-340.
[27] Mattson S S, Bartels A, Boyd A, *et al*. Continuing Analysis of Spacecraft Jitter in LROC-NAC[C]// 42st Lunar and Planetary Science Conference, The Woodlands, Texas, 2011.
[28] Wang C Y. Research on the Algorithms of High Precision Georeferencing for Space Linear Satellite Imagery[D]. Information Engineering University, 2016.
[29] Hu X B. Research on relationship of satellite flutter on-orbit versus positioning and imagery quality[D]. Wuhan University, 2013.
[30] Feng H J, Deng Q, Zheng Z Z, *et al*. Analysis of the Simulation Model Based on Remote Sensing Imaging under Vibration[J]. *Opto-Electronic Engineering*, 2013, **40**(02):1-7.
[31] Paul W R, Dewitt B A, Wilkinson B E, *et al*. Development of Collinearity Condition Equations[M/OL]. Chap. D in Elements of Photogrammetry with Applications in GIS. 4th ed. New York: McGraw-Hill Education, 2014, https://www.accessengineeringlibrary.com/content/book/9780071761123/back-matter/appendix4.
[32] Hadar O, Fisher M, Kopeika N S. Image resolution limits resulting from mechanical vibrations. Part III: numerical calculation of modulation transfer function [J]. *Optical Engineering*, 1992, **31**(3): 581-589.
[33] Wang M, Yang B, Pan J, Jin S Y. High precision geometric processing and application of high-resolution optical satellite remote sensing images[M]. Science Press, 2017.(王密, 杨博, 潘俊, 等. **高分辨率光学卫星遥感影像高精度几何处理与应用**)[M]. 科学出版社, 2017.